Regulation of transcription elongation anticipates alternative gene expression strategies across the cell cycle

Douglas Maya-Miles[1,2], José García-Martínez[3], Ildefonso Cases[4], Rocío Pasión[5], Jesús de la Cruz[1,5], José E. Pérez-Ortín[3], María de la Cruz Muñoz-Centeno[1,5], Sebastián Chávez[1,5, *]

[1]Instituto de Biomedicina de Sevilla, Universidad de Sevilla-CSIC-Hospital Universitario Virgen del Rocío, E41013 Seville, Spain.
[2]Centro de Investigación Biomédica en Red (CIBEREHD), Sevilla, Spain.
[3]Instituto de Biotecnología y Biomedicina (BIOTECMED), Facultad de Biológicas, Universitat de València. E46100 Burjassot, Spain.
[4]Unidad de Bioinformática, Centro Andaluz de Biología del Desarrollo, CSIC-Universidad Pablo de Olavide-Junta de Andalucía, E41013, Seville, Spain.
[5]Departamento de Genética, Facultad de Biología, Universidad de Sevilla, E41012 Seville, Spain.

*Corresponding author: schavez@us.es

ABSTRACT

Increasing evidence supports that the activity of RNA polymerase II (RNA pol II) during transcription elongation can be regulated to control transcription rates. Using genomic run-on (GRO) and RNA pol II chromatin immunoprecipitation (RPCC), we have respectively measured active and total RNA pol II present in the body of genes at 3 different stages of the mitotic cell cycle of *Saccharomyces cerevisiae*: G1, S and G2/M. Comparison of active and total RNA pol II values at these three points defined different patterns of transcription elongation control across the cell cycle. Previously characterized cycling genes were found associated to some of these elongation patterns. A cluster of genes with very divergent GRO and RPCC patterns was significantly enriched in genes functionally related to ribosome biogenesis (RiBi) and the structural components of the ribosome. We confirmed that RiBi mRNA expression upregulates after START but decreases after mitosis. Finally, we analysed the contribution of mRNA stability to each cluster and found that concerted control of RNA pol II activity and mRNA decay is needed to fully understand alternative strategies of gene expression across the cell cycle.

Keywords
Transcription elongation, budding yeast, ribosome biogenesis, cell cycle, *Saccharomyces cerevisiae*

INTRODUCTION

Phenotypic plasticity of living organisms is based on the control of genome expression. This regulation operates at all levels of the gene expression pathway, from gene transcription to protein degradation (reviewed in [1]). Transcription is the most regulated step in most organisms and most circumstances [2-4], although other steps play important roles under physiological dynamic changes [5].

Transcription of protein-coding genes is carried out by RNA pol II, which initiates at gene promoters, elongates pre-mRNAs along the gene bodies and terminates once pre-mRNAs are cleaved and polyadenylated. For historical reasons, most of our knowledge on transcriptional regulation deals with the initiation phase. However, in the last decades it has become evident that post-initiation regulation is an important component of genome expression control [6,7].

Regulation of transcriptional elongation in the form of promoter-proximal pausing is predominant in higher eukaryotes. In the budding yeast *Saccharomyces cerevisiae,* this mechanism does not take place, although other forms of elongation regulation operate across the genome of this yeast [8].

During elongation, RNA pol II can move backwards on its DNA template, stably blocking mRNA elongation [9]. Backtracked RNA pol II requires RNA cleavage to resume transcription [10], a molecular process that is stimulated by TFIIS [9]. Using RNA pol II ChIP (RPCC) and genomic run-on (GRO) to compare total and catalytically active molecules of elongating polymerases, respectively, we have previously shown that some gene regulons, like those related to ribosomal proteins (RP), ribosome biogenesis (RiBi) and mitochondria-related genes, are regulated at the elongation level during carbon source change, and that RP genes are particularly prone to backtracking [8].

Budding yeast genome undergoes strong changes in gene expression during the cell cycle. Approximately 10% of the *S. cerevisiae* mRNAs are expressed with cell-cycle periodicity [11]. Some reports extend this proportion until 29%, with 37% regulation at the proteomic level [12], although other studies contradict the latter (reviewed by [13]; see also [14]).

In this work, we have addressed whether regulation of RNA pol II elongation activity plays a role in this genome-wide control of gene expression across the cell cycle. Indeed, we found that it takes place in a significant proportion of the genome. Genes encoding ribosome biogenesis factors seem to be especially subject to this kind of regulation and tend to increase the proportion of active RNA pol II molecules before the onset of mitosis. Finally, we detected that distinct groups of genes showing regulated RNA pol II elongation activity also exhibit concomitant control of mRNA stability across the cell cycle, suggesting a link between these two components of gene regulation.

RESULTS

Elongating RNA pol II is highly dynamic during the cell cycle.

To determine if the activity of elongating RNA pol II undergoes changes throughout the cell cycle, we synchronized *S. cerevisiae* cells in START, released

them from the arrest and took samples for total RNA pol II (ChIP) or active RNA pol II (Genomic run-on) at 0, 30 and 60 minutes (see scheme in Figure 1A). FACS profile and budding index were used to estimate the average cell cycle stage of each sample (Figure S1). Almost all cells from samples at time 0 were in G1, whereas most cells in the 60 min samples were in G2/M. Cells from the 30 min samples were in between, with at least one third of them exhibiting the characteristic small bud of S phase, indicating a clear enrichment in this phase.
First analyses revealed many genes in which the levels of active and total RNA pol II change during the cell cycle (Figure S2A). As shown in Figure 1B, global correlation between total (RPCC) and active RNA pol II (GRO) was significant and oscillated across the cell cycle, showing a maximum R^2 value of 0.41 at the 30 min timepoint after START. When we focused in the subset of genes with significant periodic regulation across the cell cycle [15], correlation between total and active RNA pol II was slightly higher in G1 (R^2 value of 0.38 versus 0.31 in all genes) and in S-G2 (R^2 value of 0.44 versus 0.41) (Figure 1B).
Most of the categories of these cycling genes showed parallel RPCC, GRO and mRNA average profiles (Figure 1C). Using the previously published data from Eser et al [16], we also found that these transcriptional patterns were symmetrical to those of mRNA decay (Figure 1C, see later).
This parallelism between total and active RNA pol II patterns in cycling genes supports the technical consistency of our experimental data. However, some subtle differences between the RPCC and GRO average profiles were detected, particularly in the G1-S and M genes (Figure 1C). Moreover, the modest global correlation of RPCC and GRO across the genome (Figure 1B) seemed to indicate that the control of elongation dynamics might contribute to cell cycle regulation. We hypothesised that changes in gene expression during the cell cycle may result from a variety of strategies in which transcription would be regulated, not only by increasing or decreasing the number of RNA pol II molecules engaged on a gene, but also by changing their catalytic activity during elongation.

Some cycling genes are transcriptionally regulated at the elongation step

To undercover these putative regulatory strategies, we clustered all genes in 10 different groups according to their RPCC and GRO profiles along the cell cycle, following a SOTA procedure (Figures 2A and S2B). Average GRO and RPCC signals for each cluster are represented in Figure 2B, together with the mRNA expression and decay data from Eser et al [16] (see later).
Some clusters showed parallel profiles for total and active RNA pol II. For instance, cluster C exhibited marked decreases of RPCC and GRO at the 30 min timepoint followed by a limited change at 60 min (Figure 2B). A similarly simple regulation was detected in cluster G, which showed sustained increase of both RPCC and GRO signals after G1 (Figure 2B). Finally, cluster J showed peaks of both RPCC and GRO in the 30 min timepoint (Figure 2B). In all these three clusters regulation is likely exerted by controlling recruitment of RNA pol II, with little or no modulation of its elongation activity.
In contrast, the other seven clusters showed different patterns of average RPCC and GRO signals, being some of them absolutely dissimilar (Figure 2B). For instance, cluster B exhibited a marked decrease of RPCC 60 min after G1 presented a maximum of GRO at 30 min (Figure 2B). Cluster H showed increased

RPCC signals at 30 and 60 min but a flat pattern in GRO (Figure 2B). The opposite situation was found in cluster F. In this case, RPCC average signals showed some increase at 30 min whereas GRO signals dropped at this timepoint and maintained low at 60 min (Figure 2B). Cluster A exhibited a clear difference: flat RPCC profile and strong increase in GRO after G1, with a maximum at the 30 min timepoint (Figure 2B). Unparallel profiles were also detected in clusters D and I, whose RPCC signals decreased and increased, respectively, 30 min after G1, without comparable change in their GRO profiles (Figure 2B).
We wondered whether these alternative patterns of RNA pol II elongation were significant for the expression of cycling genes according to Cyclebase (Santos et al, 2014) in the ten clusters. We found significant enrichment, either positive or negative, in most of them. Particularly clear were positive enrichments found in clusters D and E (G1 genes), G (M genes), I (S/G2 and G2/M genes) and J (S, S/G2 and G2/M genes) (Figure 2C). Likewise, when we looked for the presence of our clusters in the subgroups of previously defined cycling genes, we found significant enrichment of clusters D, E and F in G1 genes, and of cluster G in M genes (Figure 2D). Interestingly, we also found a significant exclusion of all clusters but B, G, I and J from G2/M genes (Figure 2D). We also detected significant exclusion of D, E and F clusters from S/G2 genes (Figure 2D).
Interestingly, some of the clusters showing dissimilar RPCC and GRO profiles across the cell cycle, like F, D and I, were connected to cycling genes in the analyses described above. These results indicate that regulation of RNA pol II activity during ongoing transcription is compatible with cell-cycle control of gene expression and establish a first link between transcription elongation dynamics and cell cycle regulation.

Regulation of RNA pol II elongation explains the cycling pattern of RiBi genes.

We wondered whether genes contained in each cluster, in addition to a common transcriptional regulation, also shared functional similarities. Gene ontology (GO) analysis confirmed that this was the case.
As an example, cluster A was found to be enriched in terms related to ribosome biogenesis and the structural constituents of ribosomes (ribosomal proteins) (Figure 3A). These categories correspond to the RiBi and RP regulons, respectively [17] Although with lower significance, cluster A was also enriched in terms related with mRNA export and the nuclear pore (Figure 3A).
Cluster D was enriched in a wide set of categories related to respiration and metabolic pathways localized to mitochondria (Figure 3B).
Due to the particularly high significance of their GO categories, we focused in cluster A and the RiBi genes, whose regulation is critical for cell growth (reviewed in [18]; see also [19])
We investigated the cluster distribution of the 207 genes of the RiBi regulon present in our dataset and found that more than 50% belonged to cluster A, confirming the significance of this enrichment, whereas most other clusters were not enriched or even significantly depleted of this regulon (Figure 3C). All RiBi gene subgroups, including genes involved in nucleotide metabolism, translation factors and tRNA synthetases were highly represented in cluster A (Figure 3C).

We also analyzed the average GRO and RPCC profiles of all RiBi genes. As in cluster A, between the 0 and 30 min timepoints GRO signal increased more than RPCC (Figure 3D). In the case of the RP regulon less dissimilar average profiles of total and active RNA pol II were detected (Figure 3D). This lower proximity to cluster A average is explained because RP genes were not only enriched in cluster A but also in cluster G (Figure 3C), which shows similar GRO profile that cluster A but parallel to RPCC (Figure 2B). RP genes in cluster G are mainly encoding components of the large ribosomal subunit (Figure 3C). The significance of this finding is unclear, but it may reflect the existence of different mechanisms to regulate the synthesis of each ribosomal subunit.
Moreover, the differences between the RP and RiBi regulons are in agreement to the overall correlation between GRO and RPCC signals for these groups of genes across the cell cycle. While RP genes exhibited very high R^2 values in the three time points (between 0.89 and 0.94), RiBi genes showed a drastic increase in correlation from 0 (R^2 = 0.40) to 30 min (R^2 = 0.70) (Figure 3E).
Ribosome-related mRNAs has not been systematically described to undergo cyclic regulation [15], although a recent study supports periodic regulation of genes related to rRNA synthesis, cytoplasmic translation and ribosome biogenesis at the proteomic level [12]. We analyzed mRNA expression of a subset of 8 RiBi and RP genes by RT-PCR in alpha factor-synchronized cells. All analyzed RiBi exhibited peak of expression 20 min after released form alpha-factor (Fig S3). This cycling pattern was not so clear in the three RP genes analyzed (Fig S3). We conclude that most RiBi genes regulate their expression across the cell cycle in a way that involves alteration of RNA pol II activity during transcription elongation.

RNA pol II elongation patterns define alternative gene expression strategies during the cell cycle

RiBi regulon is a good example where GRO profiles anticipated mRNA expression patterns better than RPCC. In order to extend this perspective, we represented the average mRNA levels of these clusters, using the accurate transcriptomic quantitation of synchronized cells after START performed by Eser et al (2014) [16]. We confirmed that, in most cases, mRNA expression profiles followed GRO values better than RPCC (compare RPCC, GRO and mRNA expression panels in Figure 2B).
However, two clear exceptions were detected. Clusters D and I, which are enriched in G1-expressed genes, and S/G2/M genes, respectively (Figure 2C), presented closer parallelism of mRNA expression profile to RPCC than to GRO (Figure 2B). These two cases were puzzling, since RNA pol II activity measured by GRO should be a better proxy of transcription than total RNA pol II present on genes, which include backtracked RNA pol II molecules in addition to actively elongating ones [8,20-22].
In order to understand these cases, we incorporated the mRNA decay values along the cell cycle that Eser et al [16] obtained using a metabolic labelling approach. As previously described, this information facilitates to understand the regulatory behaviour of cycling genes. For instance, the decrease in mRNA expression of G1/S genes at 30 min is better explained by increased mRNA

decay than by the rather flat profile of transcriptional activity measured by GRO (Figure 1C).
This additional source of information allowed explaining the divergence between GRO and mRNA expression profiles detected in clusters D and I. We found that average mRNA decay values in cluster D were maximal at 30 min (Figure 2B). So, the combination of a mild decrease in transcriptional activity (GRO) with a marked increase in mRNA decay explains the strong downregulation of mRNA expression levels of this group of genes at the 30 min timepoint (Figure 2B).
The reverse situation took place in cluster I: mild increase in transcriptional activity (GRO), in combination with mild decrease in mRNA decay, explains a comparatively higher increase of mRNA expression at 30 min (Figure 2B). In fact, comparison of clusters I and J, which presented almost identical mRNA expression profiles, is very illustrative on two alternative strategies that produce the same average mRNA expression pattern. Whereas in cluster I, mRNA expression regulation is achieved by comparable changes in RNA pol II activity and mRNA decay, in cluster J regulation of RNA pol II activity was much more pronounced (Figure 2B). This is likely due to the overall higher stability (lower decay) of mRNAs in cluster J compared to cluster I (Figure 2B). As expected, transcriptional regulation of stable mRNAs involves more intense changes in transcriptional activity than unstable ones. GRO changes also provoked stronger alterations of mRNA expression in RiBi than in RP, which exhibited much more stable mRNAs than RiBi (Figure 3D).
Comparison of D and E clusters is also very informative. These two set of genes shared similar overall mRNA stabilities: intermediate between those of clusters I and J (Figure 2B). In this context, the stronger regulation of transcriptional activity shown by cluster E was unable to reach the regulatory effect in mRNA levels detected in cluster D, which combined milder control of transcription activity with more pronounced change of mRNA stability (Figure 2B).
A similar conclusion was obtained when we compared clusters A (stable mRNAs) and H (very unstable mRNAs): in this case, drastic upregulation of transcriptional activity with no regulation of mRNA decay (cluster A) produced the same average pattern of mRNA expression that no change in transcriptional activity combined with slight downregulation in decay (cluster H).
The synergistic effect produced by combined control of transcription and decay was also evident when we compared clusters A and G, both expressing stable mRNAs. These two clusters exhibited upregulated GRO profiles after START but, in the case of cluster G, its combination with mRNA decay downregulation provoked stronger upregulation of mRNA levels than in cluster A, where no average change of decay was detected (Figure 2B). So, in all ranges of mRNA stability most pronounced regulation of mRNA levels was achieved by concerted control of RNA pol II activity and mRNA decay.

DISCUSSION

Comparison of total RNA pol II occupancy on gene bodies by ChIP (RPCC) with transcriptional activity by genomic run-on (GRO) allowed us testing whether transcription elongation regulation may play a significant role in gene expression across the cell cycle. Only 21% of the 4764 analysed genes classified into clusters that exhibited parallel RPCC and GRO profiles after alpha factor release

(Figures 2B and S1B), indicating that most budding yeast genes undergo some kind of regulation at the RNA pol II activity level.
Several gene clusters were significantly enriched in genes previously shown to exhibit a cyclic pattern of mRNA expression. This was the case of cluster G, connected to M-specific genes (Figure 2C-D), which showed parallel RPCC, GRO and mRNA expression profiles (Figure 2B). No alteration of transcriptional activity during elongation is needed in this case to explain the regulatory behaviour of these genes.
In contrast, clusters D (enriched in G1-specific genes) and I (enriched in S-G2-M genes) showed dissimilar RPCC and GRO profiles (Figure 2B), indicating that some alterations of RNA pol II activity must take place during transcription elongation, likely by RNA pol II backtracking. In these two cases GRO profiles did not explain mRNA expression patterns, unless mRNA decay was also considered (Figure 2B, see later).
Interestingly, cluster A, which also exhibited unparallel RPCC and GRO average profiles, contained more than 50% of the RiBi gene regulon (Figure 3C). Although non-specifically described as cycling genes [15], we confirmed this regulation for some examples by RT-PCR and found a regulated mRNA expression pattern for the whole RiBi group in the cell-cycle expression dataset produced by Eser et al [16] (Figure 3D). A similar pattern, although less marked, was found for RP genes (Fig 3D), many of which were also enriched in cluster A (Figure 3C).
RNA pol II activity in RP and RiBi genes has been previously shown to be regulated during elongation in response to environmental stimuli mediated by protein kinase A [8]. Interestingly, another regulon able to modulate its elongating RNA pol II activity in response to those conditions is the one composed of genes related to respiration and other mitochondrial functions [8]. GO analyses detected significant enrichment for this kind of genes in cluster D (Figure 3B).
We have previously described that these regulons inversely change their expression in response to cell growth: mRNA concentration of RP and RiBi genes increases with growth rate, whereas that of mitochondria-related genes decreases [23]. These controls take place by different mechanisms: RP and RiBi upregulate transcription with cell growth, without changes in mRNA stability, while mitochondrial-related genes decrease mRNA stability with growth rate without significant alteration of transcription rates [23]. In agreement with this, regulation of mRNA levels in cluster A, and more specifically in RiBi and RP genes, seems to be purely transcriptional (Figures 2B and 3E), whereas cluster D mRNA expression across the cell cycle requires mRNA decay to be explained (Figure 2B).
Decreased expression of mitochondria-related genes at the 30 min time point, when at least one third of the cells were in S phase, is consistent with published evidence that indicate DNA replication occurring during the reductive phase of the *S. cerevisiae* metabolic cycle [24,25]. Increased RiBi expression at this time point is also likely related to S-phase, since nucleolus biogenesis is coupled to rDNA replication [26] and the synthesis of a whole set of new RNA pol I and ribosome components but specially biogenesis factors is required before the complete nucleolar reorganization that will take place in mitosis [27].
As discussed above, D and I are the two clusters where i) alterations of RNA pol II activity, likely by backtracking, are taking place and ii) mRNA stability is contributing to regulation. The fact that genes that have been clustered according to elongating RNA pol II activity features (RPCC/GRO profiles) exhibit clearly

distinct mRNA decay profiles, demonstrates that transcriptional elongation dynamics is important for gene expression across the cell cycle. This was particularly evident when comparing I and J clusters, which exhibit identical average mRNA expression profiles but different mRNA stabilities (Figures 2B).
A molecular connection between RNA pol II elongation dynamics and stability of the transcribed mRNA has been recently described by us for the genes controlled by the transcription factor Sfp1 [28]. During transcription of the genes undergoing this regulation, Sfp1 promotes RNA pol II backtracking until late elongation, when it is transferred from the polymerase to the nascent mRNA, which thereby become imprinted for higher stability [28]. It is tempting to hypothesize that a similar mechanism might be operating in the genes of clusters D and I. In this regard, mRNA stability of mitochondria-related genes (enriched in cluster D, Figure 2B) are controlled by Puf3, a factor which has been proposed to bind their targets co-transcriptionally [29]. In addition to Puf3-regulated ones, other genes whose mRNAs are targeted by an RNA binding protein (RBP) that influences their stability also exhibit transcriptional activation/repression, indicating the existence of specific mechanisms of crosstalk, which sum up effects on synthesis and decay rates as a way to fast regulate their targets [30].

METHODS

Cell cycle synchronization.

BY4741 S. cerevisiae cells, transformed with plasmid pRS316 to become Ura+, were grown to midlog ($O.D._{600}$ 0.25) in minimal complete (SC) medium and synchronized in G1 with 1 µg/ml of alpha factor. The percentage of unbudded cells at this stage in all three experiments was higher than 90%. Cultures were then washed in fresh media to eliminate the pheromone and released in new media. Samples for total RNA pol II (ChIP), active RNA pol II (GRO), FACS and microscopy were taken at 0, 30 and 60 minutes. To define which cell cycle stage was enriched at each time point we initially performed flow cytometry and budding index analysis. The combination of both analyses determined that at time 0 most of the cells remained in G1 (unbudded cells with or without shmoo, and a 1C DNA content) and very few had finished mitosis at 60 minutes (two differentiated nuclear masses). These two analyses are useful to discriminate the G1 (no bud or shmoo) and mid-late M (nucleus has started to split up) population but are not so efficient differentiating S, G2 and early M-phase. Median levels of total and active RNA pol II at each time point of well-established cell cycle genes [15,16] were used to better infer which cell cycle stages were enriched in each timepoint analysed (Figure 1A,C).

Genomic Run-On

Genomic run-on (GRO) was performed as described in [31] and as modified in [32]. Briefly, by macroarray hybridization, GRO detects genome-wide, active elongating RNA polymerase (RNA pol) II, whose density per gene is taken as a measurement of its synthesis rate. At the same time, the protocol allows the mRNA amounts for all the genes to be measured. mRNA half-lives are calculated as the mRNA amount/synthesis rate by assuming steady-state conditions for the

transcriptome. The total synthesis rate was calculated as the sum of the individual gene synthesis rates. 5 x 10^8 exponentially growing cells were permeabilized washing twice with 0.5% N-lauryl sarcosine sodium sulfate (sarkosyl) and recovered through low-speed centrifugation. In vivo transcription was then performed in a solution containing 120 µL of 2.5X transcription buffer (50 mM Tris-HCl pH 7.7, 500 mM KCl, 80 mM MgCl2), 16 µL of AGC mix (10 mM each of CTP, ATP, and GTP) 6 µL of DTT (0.1 M), 16 µL of [α33P] UTP (3000 Ci/mmol, 10 µCi/µL) and distilled water up to 300 µL. The mixture was incubated for 5 minutes at 30ºC to facilitate transcription elongation and halted by adding 1 mL of cold distilled water. Non-incorporated radioactive nucleotides were removed by two centrifugation wash cycles. Total RNA extraction was carried out using the Fast-Prep (Bio101 Inc.) device. Cells were resuspended in 500 µL of LETS buffer (0.1 M LiCl, 10 mM EDTA, 0.2% SDS, 10 mM Tris-HCl pH 7.4), along with 200 µL of glass beads and 500 µL of water-saturated acid phenol. Contaminants were eliminated by chloroform extraction, and labelled RNA was precipitated using 0.1 volume of 5 M LiCl and 2.5 volumes of cold ethanol for a minimum of 2 hours at -20ºC. Labelled RNA, obtained after centrifugation and washing, was spectrophotometrically quantified. All in vivo labeled RNA was utilized for hybridization (0.35-3.5 x 10^7 dpm).

Chromatin immunoprecipitation of RNA pol II (RPCC)

RPCC was performed as described in [33]. 5 x 10^8 cells were crosslinked with formaldehyde (FC 1%) for 15 minutes at room temperature. Cross-link was quenched with glycine (FC 125 mM) and washed 4 times with 30 mL ice-cold TBS buffer (20mM Tris-HCl, 140 mM NaCl, pH 7.5) and frozen. Cells were thawed on ice and resuspended in 300 µL lysis buffer [50 mM HEPES-KOH pH 7.5, 140 mM NaCl, 1 mM EDTA, 1% Triton X-100, 0.1% sodium deoxycholate, 1 mM PMSF (Phenylmethylsulfonyl fluoride), 1 mM benzamidine and 1 pill of protease inhibitor cocktail (Roche Diagnostics, Mannheim, Germany) dissolved in every 50 ml of buffer)]. The equivalent of 0.3 ml of frozen glass beads (425-600 mm; Sigma-Aldrich, St Louis, MO, USA) Cell lysis was carried out in a Fast-Prep (Bio101 Inc.) device by 2 cycles of 30 seconds. Samples were cooled down 5 minutes in ice between cycles. Samples were then sonicated in ice-cold water using a Bioruptor (Diagenode SA, Liège, Belgium) with 15´ pulses at High output (200W) during 2 cycles of 15 minutes. DNA fragments obtained ranged from 200 and 500 bp. Cell debris was removed by centrifugation at 12,000 rpm at 4°C for 5 minutes. An aliquot of 10 µL of this whole cell extract (WCE) was kept as positive control. 50 µL of Dynabeads Protein G (Dynal Invitrogen Corp., Carlsbad, CA, USA) were washed with 5 mg/ml bovine serum albumin (BSA) in PBS buffer (140 mM NaCl, 2.7 mM KCl, 10 mM Na2HPO4, 1.8 mM KH2PO4, pH 7,4) and incubated with anti-Rpb3 antibodies (ab81859; Abcam). Beads were washed with PBS/BSA to remove unbound antibody and incubated for 1.5-2 hours in agitation to enrich the samples in the DNA fragments specifically cross-linked to the RNA pol II. Beads were washed twice with lysis buffer, twice with 360 mM NaCl lysis buffer, twice with wash buffer (10 mM Tris-HCl pH 8.0, 250 mM LiCl, 0.5% Nonidet P-40, 0.5% sodium deoxycholate, 1 mM EDTA pH 8.0, 1 mM PMSF, 1 mM benzamidine and 1 pill of protease inhibitor cocktail/25 mL (Roche), and once with TE (10 mM Tris-HCl, pH 8.0, 1 mM EDTA). Two successive washes were performed with 30 µL of elution buffer (50 mM Tris-HCl pH 8.0, 10 mM EDTA, 1%

SDS) by incubating for 10 minutes at 65°C each time. The final volume of all the samples (IP, NA and WCE) was raised to 300 µL with TE and treated overnight at 65°C to reverse the cross-linking. Proteins were degraded by adding 150 µg of proteinase K for 1h 30 min at 37°C. DNA was purified using QIAquick PCR purification columns (Qiagen Inc., Valencia, CA, USA). Ligation Mediated PCR [3] was used for DNA amplification. Briefly, DNA was blunted by T4 phage DNA polymerase in a reaction volume of 124 µL (T4 DNA Pol buffer, 40 µg/µL BSA, 80 µM dNTPs, 0.6 U T4 DNA Polymerase (Roche, Basel, Switzerland). The reaction was allowed to proceed for 20 minutes at 12°C. After phenol/chloroform/isoamylic alcohol extraction, DNA was ethanol-precipitated in the presence of 12 µg of glycogen and was ligated in a final volume of 50 µL with the annealed linkers oJW102 and oJW103 (1.5 µM of each primer). The reaction was carried out overnight at 16°C and ligated DNA was precipitated and resuspended in 25 µL milliQ water. The ligated DNA was dissolved in a final volume of 40 µL (1x DNA pol buffer: 2 mM MgCl2, 0.25 mM dNTPs, 1.25 µM oligonucleotide oJW102). The reaction was started by incubating for 2 minutes at 55°C, then pausing to add 10 µL of the reaction mix (1x DNA pol buffer, 2 mM MgCl2 and 5 U DNA polymerase from Biotools, Madrid, Spain). The program was resumed for 5 minutes at 72°C, 2 minutes at 95°C and 33 cycles of 30 s at 95°C, 30 s at 55°C and 2 minutes at 72°C. DNA was precipitated overnight and resuspended in 50 µL of milliQ water. A 5 µL DNA aliquot of the LM-PCR was analyzed on a 1.2% agarose gel to check the size (average size of 300-400 bp) and PCR efficiency. The PCR product was used as a template for the radioactive labelling reaction. The reaction mixture contained 5-15 µL of amplified DNA in 50 µL (1x DNA pol buffer, 2 mM MgCl2, 0.2 mM dATP, dTTP and dGTP, 25 µM dCTP, 1 µM oJW102, 0.8 µCi/µL α-33P-dCTP and 5 U DNA polymerase). The mix was denatured for 5 minutes at 95°C, annealed 5 minutes at 50°C, and amplified for 30 minutes at 72°C. The reaction product was purified through a ProbeQuant G-50 column (Amersham Biosciences, Piscataway, NJ, USA) to remove unincorporated 33P-dCTP and oligonucleotides.

Total mRNA extraction (mRNA)

Total RNA isolated from budding yeast cells was prepared as described by Sherman et al. [34], but using a multiple-sample automated device (Fast-Prep®) to break cells.

Hybridisation, image analysis and data normalization

Nylon filters were made using PCR-amplified whole ORF sequences as probes. After pre-hybridizing nylon membranes for 1 h in 5X SSC, 5X Denhart's, 0.5% SDS, 100 µg/mL salmon sperm DNA, hybridizations were performed using 3-5 mL of the same solution containing labelled RNA. Hybridizations were conducted during 40-44 h in a roller oven at 65ºC. After hybridization, filters were washed once in 2X SSC, 0.1% SDS for 30 min, and twice in 0.2X SSC, 0.1% SDS for 30 min. Filters were exposed for up to 7 days to an imaging plate (BAS-MP, FujiFilm) which was read at 50 µm resolution in a phosphorimager scanner (FLA-3000, FujiFilm). Both GRO and RPCC experiments were performed in triplicate by swapping the filters in each replicate among the different sampling times, as described in [32] Images were quantified by using the ArrayVision 7.0 software

(Imaging Research, Inc.). The signal intensity for each spot was the background subtracted ARM Density (Artifact Removed Median). Only those values that were 1.35 times above the corresponding background were taken as valid measurements. To compare the RPCC data between experiments, the median binding ratio of the 32 rDNA spots were arbitrarily set as background. Reproducibility of the replicates was checked using the ArrayStat software (Imaging Research, Inc.). Normalization between conditions was done using the global median method for RPCC and for GRO experiments. The ratio between immunoprecipitated (IP) and whole cell extract (WCE) in each experiment (or No-Ab and WCE) after normalization was taken as the binding ratio.

Data analyses

The changes in RPCC and GRO data for all genes were evaluated by a cluster analysis of log2 transformed and z-score normalized values. It was analyzed for cluster composition with the WebMeV (Multiple Experiment Viewer) as in [35]. by means of SOTA clustering procedure. Expression data from [16] was averaged across two cycles and also z-score normalised. Decay rates from the same source was averaged across samples, log transformed and scaled to z-scores. Relation between GRO and RPCC was modelled with linear model without intercept term (Figures 1B and 3E). Values for gene categories or cycle phases (Figures 1C, 2D and 3D) were summarised by the mean; error bars represent the 95% confident interval as estimated by 1000 bootstrap resamples.

REFERENCES

[1] Pérez-Ortín, J. E., Tordera, V., & Chávez, S. (2019). Homeostasis in the Central Dogma of molecular biology: the importance of mRNA instability. RNA biology, 16(12), 1659–1666. https://doi.org/10.1080/15476286.2019.1655352

[2] Li, J. J., & Biggin, M. D. (2015). Gene expression. Statistics requantitates the central dogma. *Science (New York, N.Y.)*, *347*(6226), 1066–1067. https://doi.org/10.1126/science.aaa8332

[3] Battle, A. et al. (2015). Impact of regulatory variation from RNA to protein. Science 347, 664–667. https://doi.org/10.1126/science.1260793

[4] Jovanovic, M. et al. Immunogenetics. Dynamic profiling of the protein life cycle in response to pathogens. Science. 2015;347(6226):1259038. https://doi.org/10.1126/science.1259038

[5] Martin, B., & Suter, D. M. (2023). Gene expression flux analysis reveals specific regulatory modalities of gene expression. *iScience*, *26*(10), 107758. https://doi.org/10.1016/j.isci.2023.107758

[6] Sun, R., Fisher, R. P. (2024). The CDK9-SPT5 Axis in Control of Transcription Elongation by RNAPII. Journal of Molecular Biology (p. 168746). Elsevier BV. https://doi.org/10.1016/j.jmb.2024.168746

[7] Aoi, Y., & Shilatifard, A. (2023). Transcriptional elongation control in developmental gene expression, aging, and disease. *Molecular cell*, *83*(22), 3972–3999. https://doi.org/10.1016/j.molcel.2023.10.004

[8] Pelechano, V., Jimeno-González, S., Rodríguez-Gil, A., García-Martínez, J., Pérez-Ortín, J. E., & Chávez, S. (2009). Regulon-specific control of transcription elongation across the yeast genome. *PLoS genetics*, *5*(8), e1000614. https://doi.org/10.1371/journal.pgen.1000614

[9] Cheung, A. C., & Cramer, P. (2011). Structural basis of RNA polymerase II backtracking, arrest and reactivation. *Nature*, *471*(7337), 249–253. https://doi.org/10.1038/nature09785

[10] Sigurdsson, S., Dirac-Svejstrup, A. B., & Svejstrup, J. Q. (2010). Evidence that transcript cleavage is essential for RNA polymerase II transcription and cell viability. *Molecular cell*, *38*(2), 202–210. https://doi.org/10.1016/j.molcel.2010.02.026

[11] Bähler, J., (2005). Cell-cycle control of gene expression in budding and fission yeast. *Annual review of genetics*, *39*, 69–94. https://doi.org/10.1146/annurev.genet.39.110304.095808

[12] Campbell, K., Westholm, J., Kasvandik, S., Di Bartolomeo, F., Mormino, M., & Nielsen, J. (2020). Building blocks are synthesized on demand during the yeast cell cycle. *Proceedings of the National Academy of Sciences of the United States of America*, *117*(14), 7575–7583. https://doi.org/10.1073/pnas.1919535117

[13] No, E. G., Blank, H. M., & Polymenis, M. (2024). Patterns of protein synthesis in the budding yeast cell cycle: variable or constant?. *Microbial cell (Graz, Austria)*, *11*, 321–327. https://doi.org/10.15698/mic2024.08.835

[14] Blank, H. M., et al. (2020). Abundances of transcripts, proteins, and metabolites in the cell cycle of budding yeast reveal coordinate control of lipid metabolism. *Molecular biology of the cell, 31(10), 1069–1084*. https://doi.org/10.1091/mbc.E19-12-0708

[15] Santos, A., Wernersson, R., & Jensen, L. J. (2015). Cyclebase 3.0: a multi-organism database on cell-cycle regulation and phenotypes. *Nucleic acids research*, *43* (Database issue), D1140–D1144. https://doi.org/10.1093/nar/gku1092

[16] Eser, P., et al. (2014). Periodic mRNA synthesis and degradation co-operate during cell cycle gene expression. *Molecular systems biology*, *10*(1), 717. https://doi.org/10.1002/msb.134886

[17] Jorgensen, P., Rupes, I., Sharom, J. R., Schneper, L., Broach, J. R., & Tyers, M. (2004). A dynamic transcriptional network communicates growth potential to ribosome synthesis and critical cell size. *Genes & development*, *18*(20), 2491–2505. https://doi.org/10.1101/gad.1228804.

[18] de la Cruz, J., et al. (2018). Feedback regulation of ribosome assembly. *Current genetics*, *64*(2), 393–404. https://doi.org/10.1007/s00294-017-0764-x

[19] Gómez-Herreros, F., et al. (2017). The ribosome assembly gene network is controlled by the feedback regulation of transcription elongation. *Nucleic acids research, 45(16), 9302–9318*. https://doi.org/10.1093/nar/gkx529

[20] Rodríguez-Gil, A., et al. (2010). The distribution of active RNA polymerase II along the transcribed region is gene-specific and controlled by elongation factors. *Nucleic acids research*, *38*(14), 4651–4664. https://doi.org/10.1093/nar/gkq215

[21] Gómez-Herreros, F., de Miguel-Jiménez, L., Morillo-Huesca, M., Delgado-Ramos, L., Muñoz-Centeno, M. C., & Chávez, S. (2012). TFIIS is required for the balanced expression of the genes encoding ribosomal components under transcriptional stress. *Nucleic acids research*, *40*(14), 6508–6519. https://doi.org/10.1093/nar/gks340

[22] Jordán-Pla, A., et al. (2015). Chromatin-dependent regulation of RNA polymerases II and III activity throughout the transcription cycle. *Nucleic acids research*, *43*(2), 787–802. https://doi.org/10.1093/nar/gku1349.

[23] García-Martínez, J., Singh, A., Medina, D., Chávez, S., & Pérez-Ortín, J. E. (2023). Enhanced gene regulation by cooperation between mRNA decay and gene transcription. *Biochimica et biophysica acta. Gene regulatory mechanisms*, *1866*(2), 194910. https://doi.org/10.1016/j.bbagrm.2023.194910.

[24] Klevecz, R. R., Bolen, J., Forrest, G., & Murray, D. B. (2004). A genome-wide oscillation in transcription gates DNA replication and cell cycle. *Proceedings of the National Academy of Sciences of the United States of America*, *101*(5), 1200–1205. https://doi.org/10.1073/pnas.0306490101.

[25] Sasidharan, K., Tomita, M., Aon, M., Lloyd, D., & Murray, D. B. (2012). Time-structure of the yeast metabolism in vivo. *Advances in experimental medicine and biology*, *736*, 359–379. https://doi.org/10.1007/978-1-4419-7210-1_21

[26] Kurniawan, F., et al. (2024). Phosphorylation of Orc6 During Mitosis Regulates DNA Replication and Ribosome Biogenesis. *Molecular and cellular biology*, *44*(7), 289–301. https://doi.org/10.1080/10985549.2024.2356880

[27] Girke, P., & Seufert, W. (2019). Compositional reorganization of the nucleolus in budding yeast mitosis. *Molecular biology of the cell*, *30*(5), 591–606. https://doi.org/10.1091/mbc.E18-08-0524

[28] Kelbert, M., et al. (2024). The zinc-finger transcription factor Sfp1 imprints specific classes of mRNAs and links their synthesis to cytoplasmic decay. *eLife*, *12:RP90766.* https://doi.org/10.7554/eLife.90766.4.

[29] Garrido-Godino, A. et al.. (2021). Rpb4 and Puf3 imprint and post-transcriptionally control the stability of a common set of mRNAs in yeast. *RNA biology*, *18*(8), 1206–1220. https://doi.org/10.1080/15476286.2020.1839229

[30] García-Martínez, J., Singh, A., Medina, D., Chávez, S., & Pérez-Ortín, J. E. (2023). Enhanced gene regulation by cooperation between mRNA decay and gene transcription. *Biochimica et biophysica acta. Gene regulatory mechanisms*, *1866*(2), 194910. https://doi.org/10.1016/j.bbagrm.2023.194910

[31] García-Martínez, J., Aranda, A., & Pérez-Ortín, J. E. (2004). Genomic run-on evaluates transcription rates for all yeast genes and identifies gene regulatory mechanisms. *Molecular cell*, *15*(2), 303–313. https://doi.org/10.1016/j.molcel.2004.06.004

[32] Oliete-Calvo, P., et al. (2018). A role for Mog1 in H2Bub1 and H3K4me3 regulation affecting RNAPII transcription and mRNA export. *EMBO reports*, *19*(11), e45992. https://doi.org/10.15252/embr.201845992

[33] García-Martínez, J., Pelechano, V., & Pérez-Ortín, J. E. (2011). Genomic-wide methods to evaluate transcription rates in yeast. *Methods in molecular biology (Clifton, N.J.)*, *734*, 25–44. https://doi.org/10.1007/978-1-61779-086-7_2

[34] Sherman F, Fink GR, Hicks JB. 1986. *Methods in yeast genetics. Cold Spring Harbor, NY: Cold Spring Harbor Laboratory*

[35] Romero, A. M., et al. (2019). A genome-wide transcriptional study reveals that iron deficiency inhibits the yeast TORC1 pathway. *Biochimica et biophysica acta. Gene regulatory mechanisms*, *1862*(9), 194414. https://doi.org/10.1016/j.bbagrm.2019.194414

Acknowledgements

We thank all members of the IBiS Gene expression and Ribosome biogenesis labs for helpful scientific discussion, and all technicians from IBiS and CITIUS facilities for their experimental help. This work was supported by grants PID2020-112853GB-C31 to JEP-O, PID2022-136564NB-I00 to JdlC and PID2020-112853GB-C32 to MCM-C funded by MCIN/AEI/10.13039/501100011033/ERDF, EU.

Author contributions

In this work, D. Maya-Miles performed most of the experiments, analysed the data, and contributed to the design and writing of the manuscript. J. García-Martínez performed some experiments, handled the original transcriptomic data, and performed some preliminary analyses. R. Pasión performed experiments. I Cases performed most of the bioinformatic analysis. J. de la Cruz and J.E. Pérez-Ortín guided the experimental design

and contributed to the writing. M.C. Muñoz-Centeno supervised the experimental work, guided the experimental design and contributed to the writing. S. Chávez guided the experimental design, drafted the manuscript and checked its final version. All authors read and approved the final manuscript.

Data availability statement

Data produced in the experiments described in this work are publicly available in the Gene Expression Omnibus repository (GSE277924). Reviewers and editors can access the data using the following private token: cpyzygggxdglfqr.

Competing Interests

The authors declare no competing interests.

Figure legends

Figure 1: Distribution of total and active RNA polymerase II at genes during the transition from G1 to G2. A) Schematic representation of times and samples taken for the analysis of total and active RNA pol II. B) Plot representing total (RPCC) and active RNA pol II (GRO) present in each gene at each time point analysed. Black line: Overall tendency. Dashed blue line: Cycling genes. C) Behaviour of total (RPCC) and active RNA pol II (GRO) using CycleBase 3.0 as reference. Total mRNA expression and mRNA decay values from Eser et al [16] are also represented.

Figure 2: Clustering analysis of total and active RNA pol II at genes during the transition from G1 to G2. A) Overview of the different clusters identified with SOTA analysis. B) Behaviour of total RNA pol II (RPCC), active RNA pol II (GRO) in each cluster identified. mRNA expression and mRNA decay data from Eser et al [16] are also represented. C) Distribution of cell cycle genes according to their peak of maximal expression (CellCycle Base 3.0) in each of the clusters identified. D) Distribution of identified clusters within the different categories of cell cycle genes according to their peak of maximal accumulation (CellCycle Base 3.0). Green arrows represent groups in which the enrichment or depletion of cell cycle genes (C) or clusters (D) is statistically significant (logistic regression with BF correction).

Figure 3: Cell cycle and functional analysis of total and active RNA pol II across the cell cycle. A) Gene ontology analysis with gProfiler of cluster A-containing genes. B) Similar for cluster -containing genes. C) Distribution of identified clusters and logistic regression analyses within RIBI and subcategories (upper section) and within RP genes and subcategories (lower section). D) Representation of total and active RNA pol II in RIBi and RP genes. mRNA expression and mRNA decay data from Eser et al [16] are also

represented. E) Normalized values for all (grey), RIBI (red) and RP (green) genes, for total (RPCC) and active RNA pol II (GRO).

A.

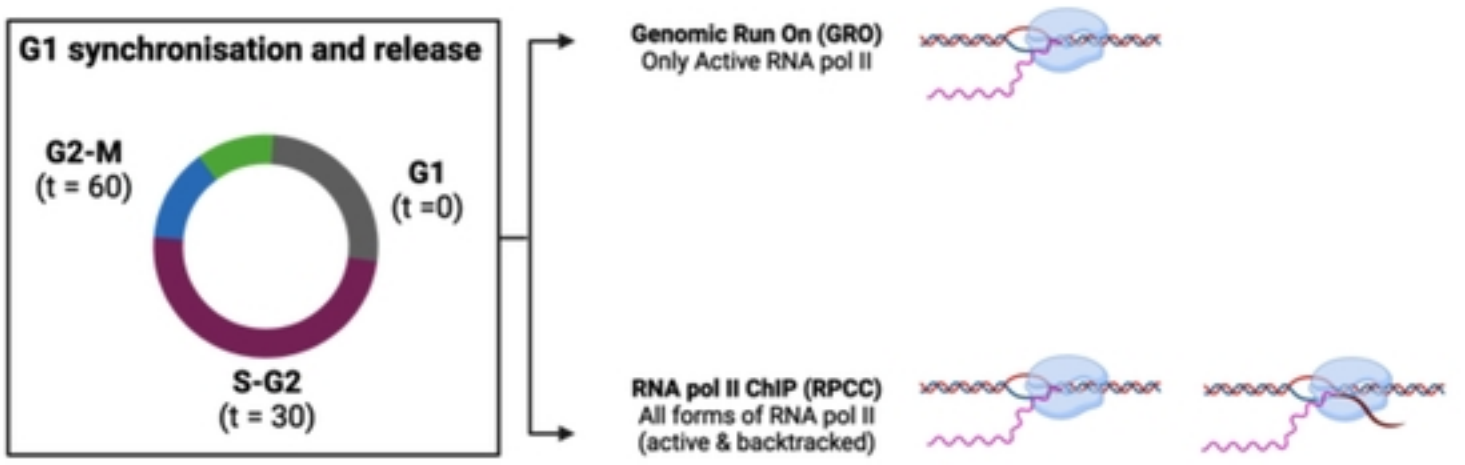
G1 synchronisation and release
G2-M
(t = 60)
G1
(t =0)
S-G2
(t = 30)
Genomic Run On (GRO)
Only Active RNA pol II
RNA pol II ChIP (RPCC)
All forms of RNA pol II
(active & backtracked)

B.

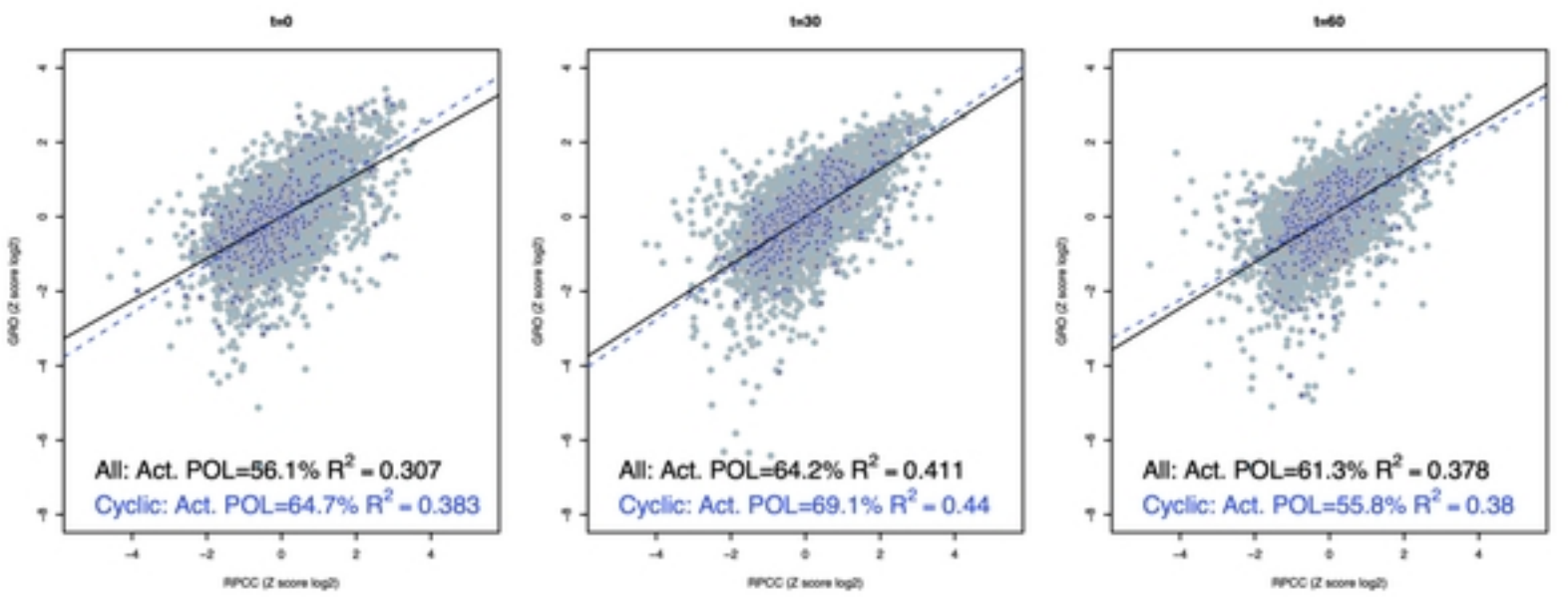
t=0
t=30
t=60
All: Act. POL=56.1% R² = 0.307
Cyclic: Act. POL=64.7% R² = 0.383
All: Act. POL=64.2% R² = 0.411
Cyclic: Act. POL=69.1% R² = 0.44
All: Act. POL=61.3% R² = 0.378
Cyclic: Act. POL=55.8% R² = 0.38

C.

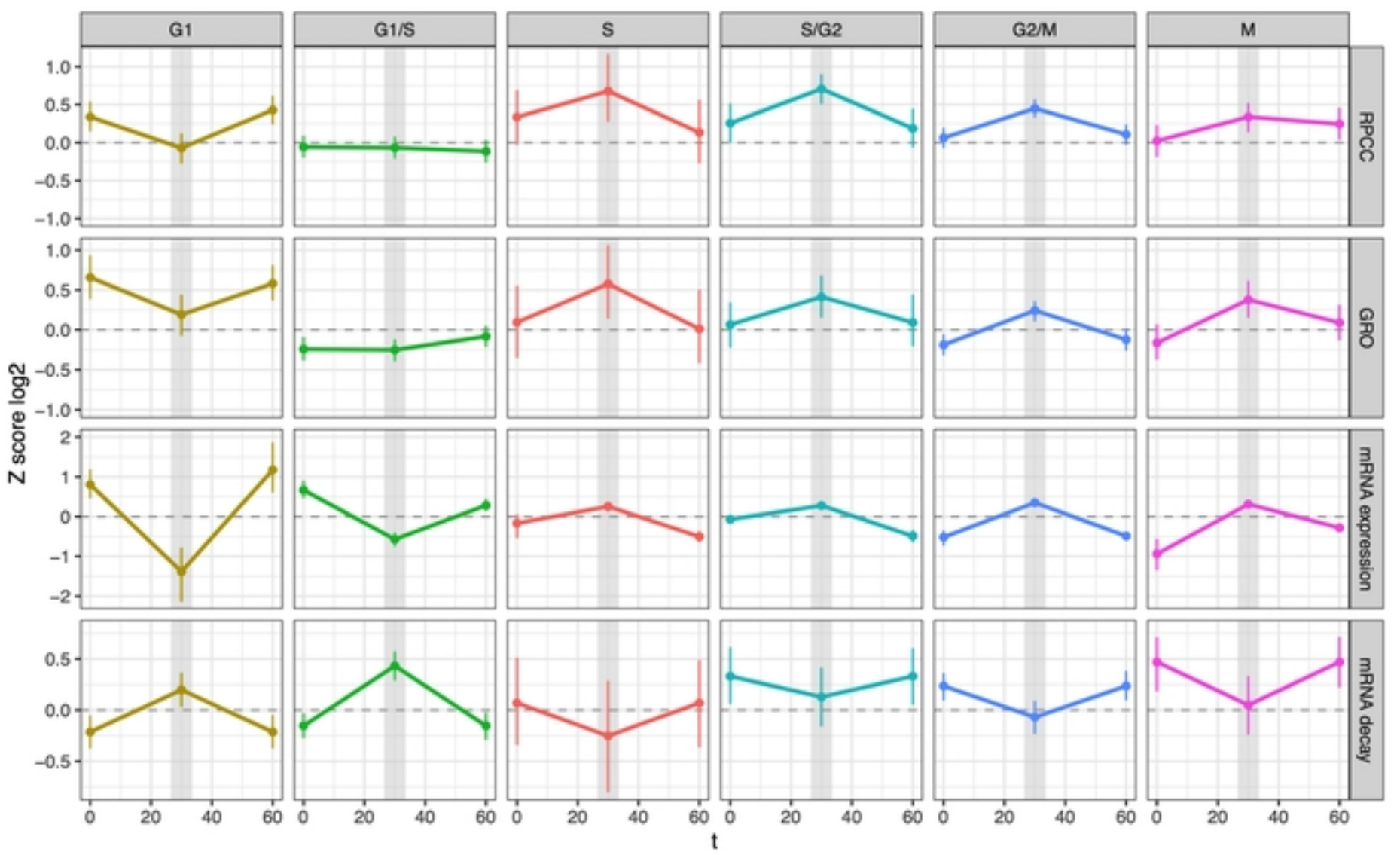
G1
G1/S
S
S/G2
G2/M
M
RPCC
GRO
mRNA expression
mRNA decay
Z score log2
t

Figure 1

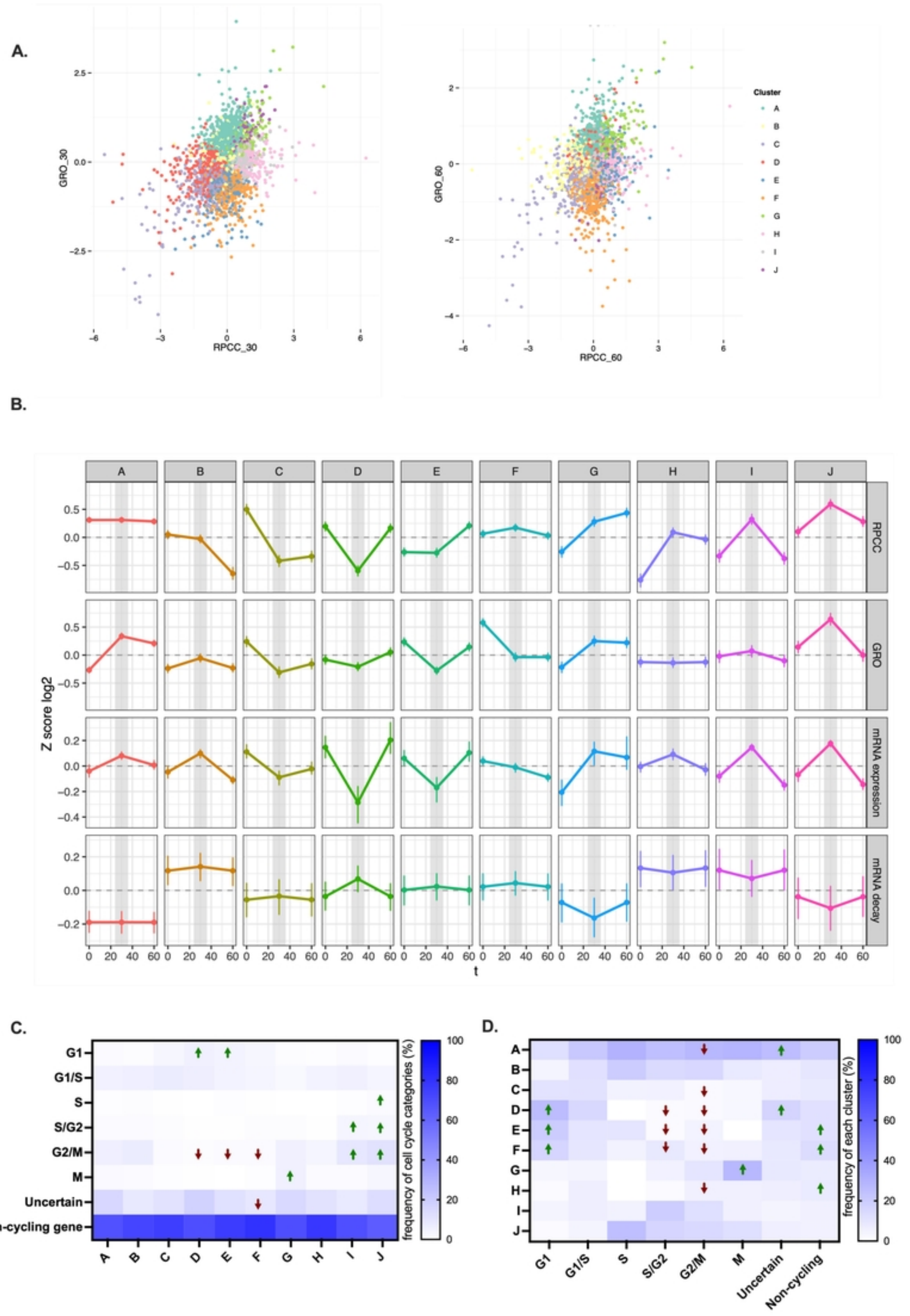
A.
GRO_30
RPCC_30
GRO_60
RPCC_60
Cluster
A
B
C
D
E
F
G
H
I
J
B.
Z score log2
RPCC
GRO
mRNA expression
mRNA decay
t
C.
G1
G1/S
S
S/G2
G2/M
M
Uncertain
Non-cycling gene
frequency of cell cycle categories (%)
D.
frequency of each cluster (%)
Non-cycling

Figure 2

A.

Term ID	Term Name	p_{adj} (query_1) ↑
GO:0042254	ribosome biogenesis	3.879×10^{-34}
GO:0032991	protein-containing complex	4.802×10^{-29}
GO:0005488	binding	4.464×10^{-20}
GO:0043412	macromolecule modification	1.560×10^{-10}
GO:0003735	structural constituent of ribosome	6.916×10^{-5}
GO:0140098	catalytic activity, acting on RNA	1.510×10^{-4}
GO:0071042	nuclear polyadenylation-dependent mRNA cat...	6.064×10^{-3}
GO:0071051	polyadenylation-dependent snoRNA 3'-end pr...	6.064×10^{-3}
GO:0009156	ribonucleoside monophosphate biosynthetic pr...	6.605×10^{-3}
GO:0008170	N-methyltransferase activity	8.650×10^{-3}
GO:0004298	threonine-type endopeptidase activity	9.054×10^{-3}
GO:0043021	ribonucleoprotein complex binding	1.107×10^{-2}
GO:0051028	mRNA transport	2.655×10^{-2}
GO:0006450	regulation of translational fidelity	2.829×10^{-2}
GO:0051664	nuclear pore localization	3.334×10^{-2}
GO:0010494	cytoplasmic stress granule	4.081×10^{-2}

B.

Term ID	Term Name	p_{adj} (query_1)
GO:0016491	oxidoreductase activity	3.892×10^{-3}
GO:0016743	carboxyl- or carbamoyltransferase activity	1.291×10^{-2}
GO:0009055	electron transfer activity	4.596×10^{-2}
GO:0008652	amino acid biosynthetic process	3.904×10^{-4}
GO:0009084	glutamine family amino acid biosynthetic proce...	1.663×10^{-3}
GO:0009987	cellular process	1.006×10^{-2}
GO:0042773	ATP synthesis coupled electron transport	1.210×10^{-2}
GO:0098798	mitochondrial protein-containing complex	1.416×10^{-4}
GO:0005759	mitochondrial matrix	2.736×10^{-3}
GO:0005622	intracellular anatomical structure	5.570×10^{-3}
GO:0005750	mitochondrial respiratory chain complex III	2.516×10^{-2}
GO:0031090	organelle membrane	2.919×10^{-2}
GO:0070469	respirasome	4.943×10^{-2}

C.

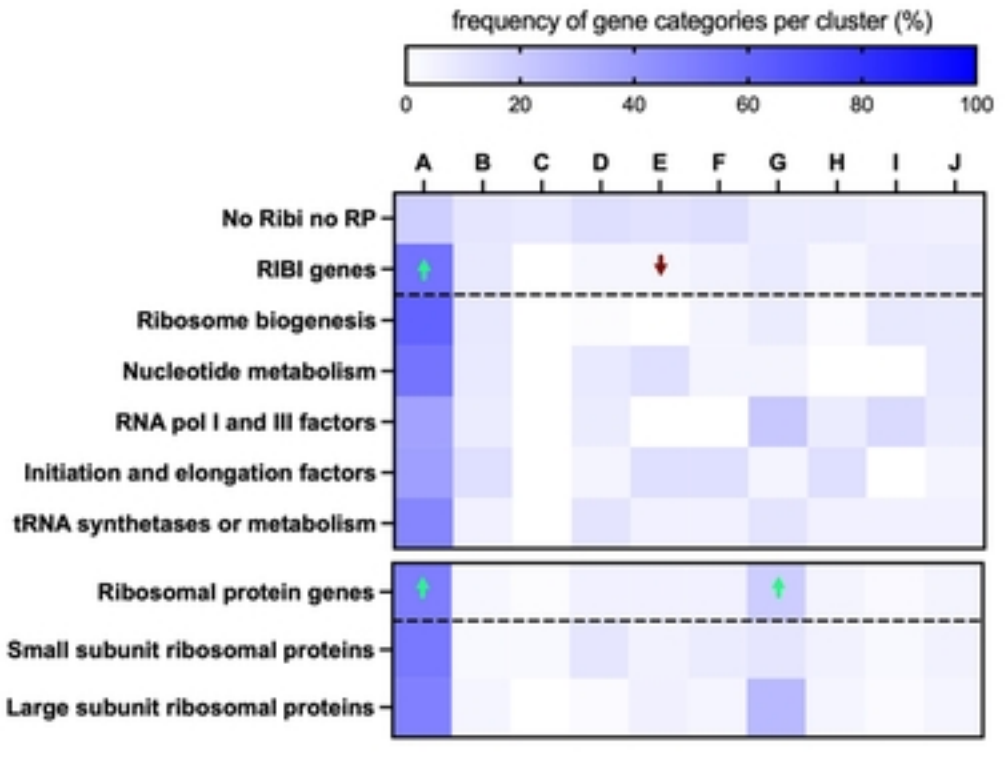

D.

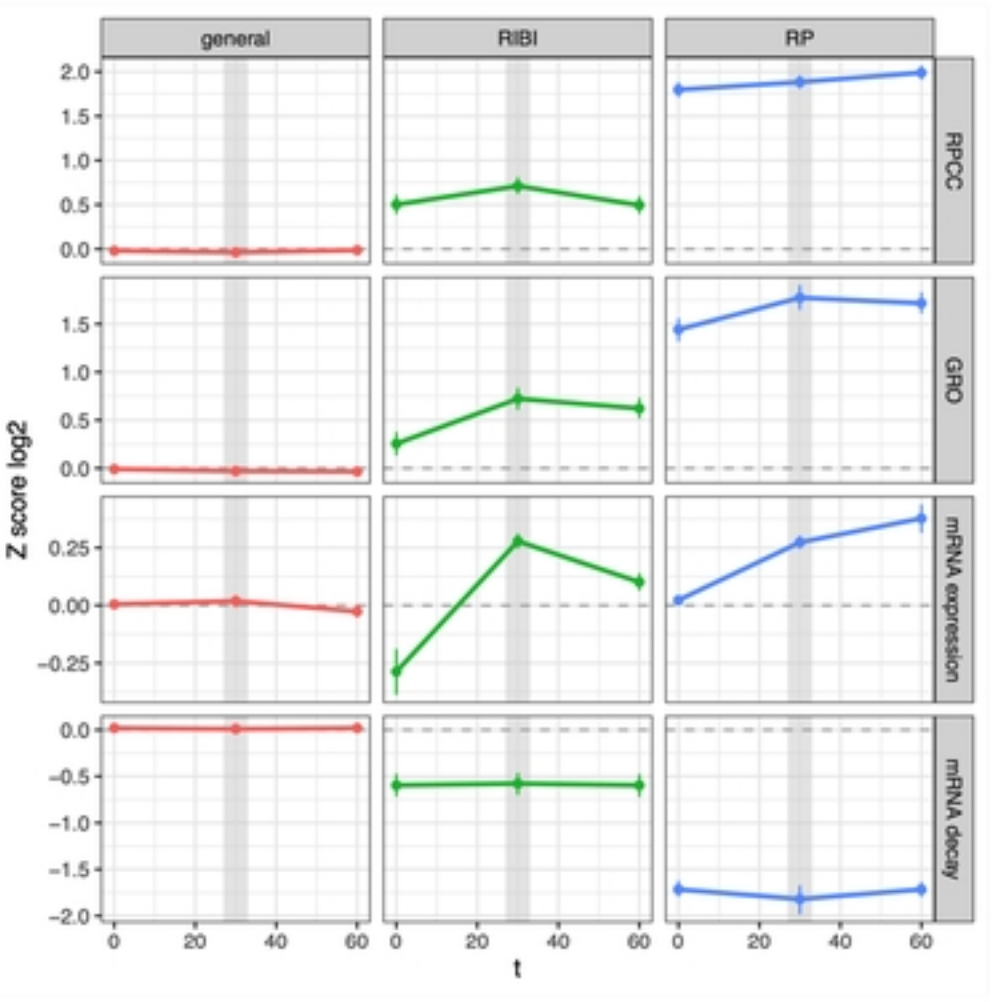

E.

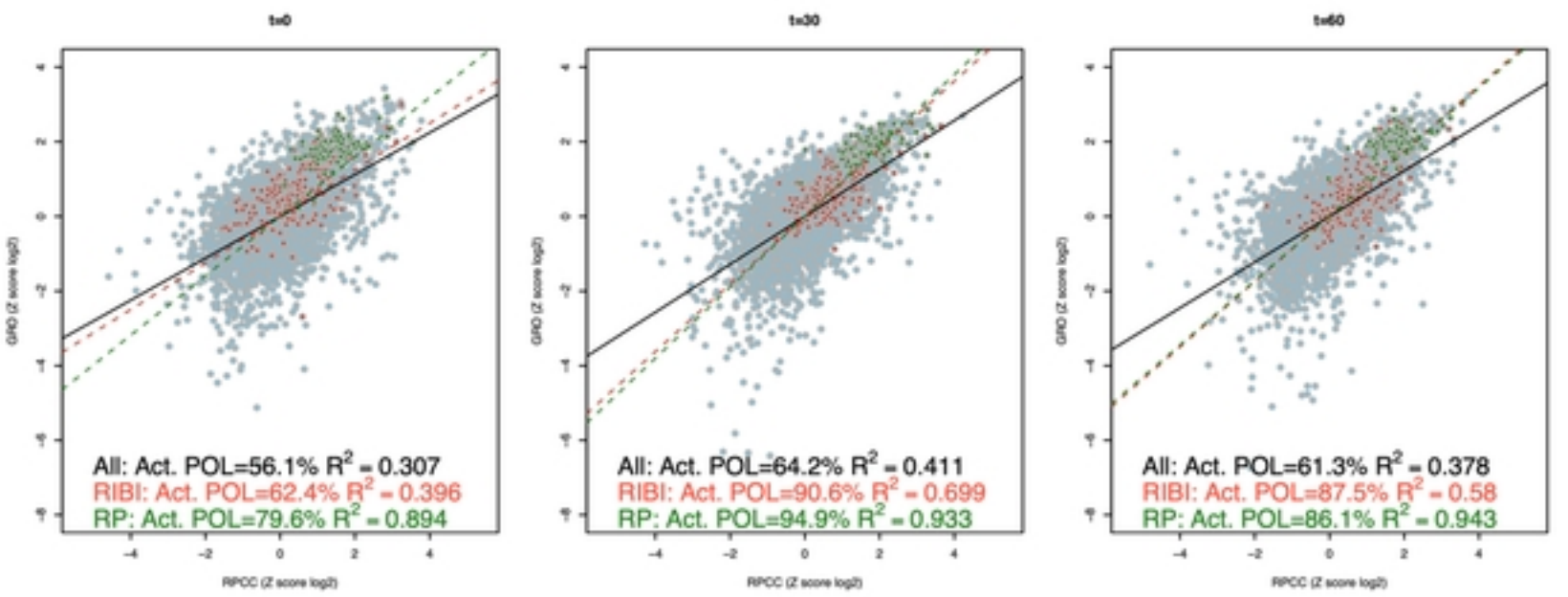

Figure 3